PHYSICAL REVIEW D **80,** 054009 (2009)

Measuring the running top-quark mass

U. Langenfeld,[1] S. Moch,[1] and P. Uwer[2]

[1]*Deutsches Elektronensynchrotron DESY, Platanenallee 6, D15738 Zeuthen, Germany*

[2]*Institut für Physik, Humboldt-Universität zu Berlin, Newtonstraße 15, D12489 Berlin, Germany*

(Received 9 July 2009; published 9 September 2009)

We present the first direct determination of the running top-quark mass based on the total cross section of top-quark pair production as measured at the Tevatron. Our theory prediction for the cross section includes various next-to-next-to-leading order QCD contributions, in particular, all logarithmically enhanced terms near threshold, the Coulomb corrections at two loops and all explicitly scale-dependent terms at next-to-next-to-leading order accuracy. The result allows for an exact and independent variation of the renormalization and factorization scales. For Tevatron and LHC we study its dependence on all scales, on the parton luminosity and on the top-quark mass using both the conventional pole mass definition as well as the running mass in the $\overline{\mathrm{MS}}$ scheme. We extract for the top quark an $\overline{\mathrm{MS}}$ mass of $m(\mu = m) = 160.0^{+3.3}_{-3.2}$ GeV, which corresponds to a pole mass of $m_t = 168.9^{+3.5}_{-3.4}$ GeV.

DOI: 10.1103/PhysRevD.80.054009 PACS numbers: 12.38.Bx, 13.85.Ni

I. INTRODUCTION

The top quark is the heaviest elementary particle discovered so far and it is likely to be the most sensitive probe of the electroweak symmetry breaking. This is reflected in the fact that in many extensions of the standard model the top quark plays a special role. The precise measurement of top-quark properties is thus an important task for the Large Hadron Collider (LHC) (see e.g. Refs. [1,2]). One of the most basic quantities in that respect is the total cross section which is currently measured at the Tevatron and will be measured at the LHC. The precise measurements aimed for at the LHC are asking for an equally precise theoretical prediction to compare with. In this paper, we update and extend the predictions of Refs. [3,4] for the total hadronic cross section of top-quark pairs and its associated theoretical uncertainty. Related recent studies have also appeared in Refs. [5–7]. As a novel aspect of this paper, we employ the $\overline{\mathrm{MS}}$ definition for the top-quark mass and present the total cross section as a function of the running mass. This allows the direct determination of an $\overline{\mathrm{MS}}$ mass from Tevatron measurements for the total cross section [8].

We start by recalling the relevant formulas for the total cross section of top-quark hadroproduction within perturbative quantum chromodynamics (QCD):

$$\sigma_{pp\to t\bar{t}X}(S, m_t^2) = \frac{\alpha_s^2}{m_t^2} \sum_{i,j=q,\bar{q},g} \int_{4m_t^2}^{S} ds L_{ij}(s, S, \mu_f^2) f_{ij}(\rho, M, R), \tag{1}$$

$$L_{ij}(s, S, \mu_f^2) = \frac{1}{S} \int_s^S \frac{d\hat{s}}{\hat{s}} \phi_{i/p}\left(\frac{\hat{s}}{S}, \mu_f^2\right) \phi_{j/p}\left(\frac{s}{\hat{s}}, \mu_f^2\right), \tag{2}$$

where S and m_t denote the hadronic center-of-mass energy squared and the top-quark mass (here taken to be the pole mass), respectively, while L_{ij} is the usual definition of the parton luminosity with the parton distributions (PDFs) $\phi_{i/p}$ at the factorization scale μ_f. The scaling functions f_{ij} parametrize the hard partonic scattering process. They depend only on dimensionless ratios of m_t, μ_f, the renormalization scale μ_r and the partonic center-of-mass energy squared s, with the definitions $\rho = 4m_t^2/s$, $R = \mu_r^2/\mu_f^2$ and $M = \mu_f^2/m_t^2$. The radiative corrections to the scaling functions f_{ij} at the next-to-leading order (NLO) [9–11] are long known and recently even the complete analytic expressions have become available [12]. In order to quantify the theory uncertainty also the next-to-next-to-leading order (NNLO) must be included. Presently, these NNLO corrections [3,4] are approximated by the complete tower of the Sudakov logarithms and including all two-loop Coulomb corrections.

In the present study we include consistently the channels, $q\bar{q}$, gg and gq through NNLO and we provide parametrizations for all necessary scaling functions in the standard $\overline{\mathrm{MS}}$ scheme for mass factorization. This allows for an easy handling in phenomenological applications. Our phenomenological study reflects the latest measured value for the top-quark mass [13], $m_t = 173.1^{+1.3}_{-1.3}$ GeV, and employs new PDF sets [7,14]. Let us briefly summarize the key aspects of our update with respect to Refs. [3,4]:

(i) We use exact dependence on the renormalization and factorization scale. This allows for an independent variation of μ_r and μ_f (extending Ref. [15]) and is commonly considered as more reliable to establish the theoretical uncertainty of perturbative predictions (see e.g. Ref. [16]).

(ii) We perform the singlet-octet color decomposition consistently when matching our threshold expansion at NLO using results of Refs. [17–19]. The numerical impact on phenomenology at LHC and Tevatron turns out to be negligible, though.

(iii) We discuss those residual systematical uncertainties of our predictions for LHC and Tevatron, which are inherent in the approach based on threshold resummation and we comment on the size of unknown corrections.

(iv) We quantify the numerical impact of other known effects on the total cross section, such as the electroweak radiative corrections at NLO [20–22] and bound state corrections in QCD at threshold [18,19].

(v) We study the dependence of the total cross section on the definition of the mass parameter. For the conversion of the conventionally used pole mass m_t [see Eq. (1)] and the scale-dependent $\overline{\text{MS}}$ mass $m(\mu_r)$ we exploit well-known relations to NNLO [23] (see also Refs. [24,25]). We investigate the apparent convergence of both definitions, m_t and $m(\mu_r)$, in perturbation theory through NNLO.

We also employ the analytic results for the NLO scaling functions [12]. As a net effect these lead to small improvements in the gq- and the gg-channel contributions of our NNLO prediction.

II. THEORETICAL SETUP

The perturbative expansion of the scaling functions f_{ij} in the strong coupling α_s up to two loops around $M = R = 1$, i.e. $m_t = \mu_r = \mu_f$, reads

$$f_{ij}(\rho, 1, 1) = f_{ij}^{(0)}(\rho) + 4\pi\alpha_s f_{ij}^{(10)}(\rho) + (4\pi\alpha_s)^2 f_{ij}^{(20)}(\rho), \tag{3}$$

and the functions $f_{ij}^{(0)}$, $f_{ij}^{(10)}$ and $f_{ij}^{(20)}$ contain, at each order in α_s, genuinely new information to be calculated from first principles in perturbation theory. At the Born level,

$$f_{q\bar{q}}^{(0)} = \frac{\pi\beta\rho}{27}[2 + \rho], \tag{4}$$

$$f_{gq}^{(0)} = 0, \tag{5}$$

$$f_{gg}^{(0)} = \frac{\pi\beta\rho}{192}\left[\frac{1}{\beta}(\rho^2 + 16\rho + 16)\ln\left(\frac{1+\beta}{1-\beta}\right) - 28 - 31\rho\right], \tag{6}$$

where β is the heavy quark velocity with $\beta = \sqrt{1-\rho}$. At NLO the known functions $f_{ij}^{(10)}$ can be described through parametrizations which are accurate at the per mille level. Our one-loop fits use the following ansatz:

$$f_{q\bar{q}}^{(10)} = \frac{\rho\beta}{36\pi}\left[\frac{32}{3}\ln^2\beta + \left(32\ln 2 - \frac{82}{3}\right)\ln\beta - \frac{1}{12}\frac{\pi^2}{\beta}\right] + \beta\rho a_0^{qq} + h(\beta, a_1, \ldots, a_{17}) + \frac{1}{8\pi^2}(n_f - 4) f_{q\bar{q}}^{(0)}\left[\frac{4}{3}\ln 2 - \frac{2}{3}\ln\rho - \frac{10}{9}\right], \tag{7}$$

$$f_{gq}^{(10)} = \frac{1}{16\pi}\beta^3\left[\frac{5}{9}\ln\beta + \frac{5}{6}\ln 2 - \frac{73}{108}\right] + h_{gq}^{(a)}(\beta, a_1, \ldots, a_{15}), \tag{8}$$

$$f_{gg}^{(10)} = \frac{7\beta}{768\pi}\left[24\ln^2\beta + \left(72\ln 2 - \frac{366}{7}\right)\ln\beta + \frac{11}{84}\frac{\pi^2}{\beta}\right] + \beta a_0^{gg} + h(\beta, a_1, \ldots, a_{17}) + (n_f - 4)\frac{\rho^2}{1024\pi} \times \left[\ln\left(\frac{1+\beta}{1-\beta}\right) - 2\beta\right], \tag{9}$$

where n_f denotes the number of light quarks and we have kept the complete dependence on n_f in all parametrizations manifest. The Sudakov logarithms $\ln\beta$ at threshold and the Coulomb corrections ($\sim 1/\beta$) in Eqs. (7)–(9) are exact [9]. The constants a_0^{ij} read

$$a_0^{qq} = \frac{299}{324\pi} - \frac{43}{1296}\pi - \frac{121}{108}\frac{\ln 2}{\pi} + \frac{16}{27}\frac{\ln^2 2}{\pi} \approx 0.032\,947\,34, \tag{10}$$

$$a_0^{gg} = \frac{1111}{2304\pi} - \frac{283}{18\,432}\pi - \frac{89}{128}\frac{\ln 2}{\pi} + \frac{7}{16}\frac{\ln^2 2}{\pi} \approx 0.018\,752\,87. \tag{11}$$

They are known from the computation of the NLO QCD corrections to hadroproduction of quarkonium [17] (see also Refs. [18,19]), where also details of the decomposition of a_0^{gg} for color-singlet and color-octet states can be found. The constants a_0^{ij} in Eqs. (10) and (11) emerge from Refs. [17–19] by means of a simple Mellin transformation and agree with the values quoted in Ref. [12]. The coefficients of the functions $h(\beta, a_1, \ldots, a_{17})$ and $h_{gq}^{(a)}(\beta, a_1, \ldots, a_{15})$ in Eqs. (7)–(9) are determined in a fit to the analytic expressions of Ref. [12]. Near threshold we have $h(\beta) = \mathcal{O}(\beta^2)$. More details are given in Eqs. (A7) and (A8). Because of the larger number of parameters in the fit functions, it is evident that Eqs. (7)–(9) supersede earlier parametrizations [9] with respect to accuracy.

At the two-loop level we know the complete tower of Sudakov logarithms, $\ln^k\beta$ with $k = 1, \ldots, 4$, for the functions $f_{q\bar{q}}^{(20)}$ and $f_{gg}^{(20)}$ and, in addition, also the complete Coulomb contributions, $\sim 1/\beta^2$, $1/\beta$. The channel gq is power suppressed near threshold relative to $q\bar{q}$ and gg. However, extending soft gluon resummation to power suppressed quantities (see e.g. Refs. [26,27]) and using Eq. (8), we can determine (at least) the leading term $\sim\ln^3\beta$ of the function $f_{gq}^{(20)}$. We find

$$f_{q\bar{q}}^{(20)} = \frac{f_{q\bar{q}}^{(0)}}{(16\pi^2)^2}\Bigg[\frac{8192}{9}\ln^4\beta + \left(-\frac{15\,872}{3} + \frac{16\,384}{3}\ln 2 + \frac{1024}{27}n_f\right)\ln^3\beta + \left(1046.4831 - 90.838\,135 n_f - 140.367\,71\,\frac{1}{\beta}\right)\ln^2\beta + \Bigg(1029.8687 - 2.890\,391\,9 n_f - 2D_{Q\bar{Q}}^{(2)} + (54.038\,454 - 4.386\,490\,8 n_f)\frac{1}{\beta}\Bigg)\ln\beta + 3.607\,744\,1\,\frac{1}{\beta^2} + (7.399\,696\,3 + 0.614\,925\,28 n_f)\frac{1}{\beta} + C_{q\bar{q}}^{(2)}\Bigg], \quad (12)$$

$$f_{gq}^{(20)} = \frac{\beta^3}{(16\pi^2)^2}\,\frac{65\pi}{54}\ln^3(8\beta^2), \quad (13)$$

$$f_{gg}^{(20)} = \frac{f_{gg}^{(0)}}{(16\pi^2)^2}\Bigg[4608\ln^4\beta + \left(-\frac{150\,400}{7} + 27\,648\ln 2 + \frac{256}{3}n_f\right)\ln^3\beta + \left(-315.572\,18 - 119.355\,29 n_f + 496.300\,11\,\frac{1}{\beta}\right)\ln^2\beta + \Bigg(3249.2403 - 19.935\,233 n_f - 1.428\,571\,4 D_{Q\bar{Q}}^{(2)} + (286.671\,32 + 6.893\,057\,0 n_f)\frac{1}{\beta}\Bigg)\ln\beta + 68.547\,138\,\frac{1}{\beta^2} - (192.100\,86 + 0.966\,311\,15 n_f)\frac{1}{\beta} + C_{gg}^{(2)}\Bigg]. \quad (14)$$

Equations (12) and (14) are exact up to the unknown constant terms $C_{q\bar{q}}^{(2)}$ and $C_{gg}^{(2)}$ of order $\mathcal{O}(\beta^0)$, whereas Eq. (13) receives further corrections of order $\mathcal{O}(\beta^3\ln^2\beta)$. Please note that the numerical coefficients in Eqs. (12) and (14) have slightly changed compared to Ref. [3]. The $\ln^2\beta$ terms in Eqs. (12) and (14) are affected by using the exact coefficients (10) and (11) in the matching at NLO. The linear terms proportional to $\ln\beta$ in Eqs. (12) and (14) contain genuine two-loop contributions. Among those is the soft anomalous dimension $D_{Q\bar{Q}}^{(2)}$ (see Ref. [3]). Inserting the respective numerical coefficients we find $730.739\,16 + 23.776\,275 n_f$ in Eq. (12) and $3035.5764 - 0.887\,613\,78 n_f$ in Eq. (14). The latter value has changed with respect to Ref. [3] due to a consistent separation of the color-singlet and color-octet contributions in a_0^{gg} at NLO [17–19]. However the phenomenology is rather insensitive to this change and is only affected at the per mille level. The Coulomb terms ($\sim 1/\beta$) in Eqs. (12) and (14) contain all contributions from the two-loop virtual corrections. Equation (13) gives the leading (though formally power suppressed) contribution at two loops to the gq channel. We include $f_{gq}^{(20)}$ in our analysis for three reasons. First, under evolution of the factorization scale the gq channel mixes with the two other channels and for a consistent study of the factorization scale dependence this channel also needs to be taken into account. Next, the luminosity L_{gq} in particular at LHC is sizable and Eq. (13) offers a way to control its numerical impact at higher orders. Finally, Eq. (13) provides a first step towards a general study of power suppressed but logarithmically enhanced terms near threshold for top-quark production.

In Eq. (1) the dependence of the scaling functions f_{ij} on the renormalization and factorization scales, μ_r and μ_f, respectively, can also be made explicit. Starting from the expansion in α_s through NNLO around $R = 1$, i.e. $\mu_r = \mu_f$, we introduce

$$f_{ij}(\rho, M, 1) = f_{ij}^{(0)}(\rho) + 4\pi\alpha_s\{f_{ij}^{(10)}(\rho) + L_M f_{ij}^{(11)}(\rho)\} + (4\pi\alpha_s)^2\{f_{ij}^{(20)}(\rho) + L_M f_{ij}^{(21)}(\rho) + L_M^2 f_{ij}^{(22)}(\rho)\}, \quad (15)$$

where we abbreviate $L_M = \ln(\mu_f^2/m_t^2)$. The logarithmic tower in $M = \mu_f^2/m_t^2$, that is, all terms proportional to L_M in Eq. (15), can be derived by renormalization group methods in a straightforward manner. The explicit results in the $\overline{\text{MS}}$ scheme for all channels read at NLO

$$f_{ij}^{(11)} = -(2P_{ij}^{(0)} - 2\beta_0\mathbb{1}) \otimes f_{ij}^{(0)}, \quad (16)$$

$$f_{gq}^{(11)} = -P_{gq}^{(0)} \otimes f_{gg}^{(0)} - \frac{1}{2n_f}P_{qg}^{(0)} \otimes f_{q\bar{q}}^{(0)}, \quad (17)$$

where $ij = \{q\bar{q}, gg\}$ in Eq. (16). At NNLO we have

$$f_{q\bar{q}}^{(21)} = -(2P_{qq}^{(1)} - 2\beta_1\mathbb{1}) \otimes f_{q\bar{q}}^{(0)} - (2P_{qq}^{(0)} - 3\beta_0\mathbb{1}) \otimes f_{q\bar{q}}^{(10)} - 2P_{gq}^{(0)} \otimes f_{gq}^{(10)}, \quad (18)$$

$$f_{q\bar{q}}^{(22)} = \left(2P_{qq}^{(0)} \otimes P_{qq}^{(0)} - 5P_{qq}^{(0)}\beta_0 + \frac{1}{2n_f}P_{qg}^{(0)} \otimes P_{gq}^{(0)} + 3\beta_0^2\mathbb{1}\right) \otimes f_{q\bar{q}}^{(0)} + P_{gq}^{(0)} \otimes P_{gq}^{(0)} \otimes f_{gg}^{(0)}, \quad (19)$$

$$f_{gq}^{(21)} = -\frac{1}{2n_f}P_{qg}^{(0)} \otimes f_{q\bar{q}}^{(10)} - (P_{qq}^{(0)} + P_{gg}^{(0)} - 3\beta_0\mathbb{1}) \otimes f_{gq}^{(10)} - P_{gq}^{(1)} \otimes f_{gg}^{(0)} - \frac{1}{2n_f}P_{qg}^{(1)} \otimes f_{q\bar{q}}^{(0)} - P_{gq}^{(0)} \otimes f_{gg}^{(10)}, \quad (20)$$

$$f_{gq}^{(22)} = \frac{1}{4n_f} P_{qg}^{(0)} \otimes (3P_{qq}^{(0)} + P_{gg}^{(0)} - 5\beta_0 \mathbb{1}) \otimes f_{q\bar{q}}^{(0)} + \frac{1}{2} P_{gq}^{(0)} \otimes (P_{qq}^{(0)} + 3P_{gg}^{(0)} - 5\beta_0 \mathbb{1}) \otimes f_{gg}^{(0)}, \tag{21}$$

$$f_{gg}^{(21)} = -(2P_{gg}^{(1)} - 2\beta_1 \mathbb{1}) \otimes f_{gg}^{(0)} - (2P_{gg}^{(0)} - 3\beta_0 \mathbb{1}) \otimes f_{gg}^{(10)} - 2P_{qg}^{(0)} \otimes f_{gq}^{(10)}, \tag{22}$$

$$f_{gg}^{(22)} = \frac{1}{2n_f} P_{qg}^{(0)} \otimes P_{qg}^{(0)} \otimes f_{q\bar{q}}^{(0)} + (P_{qg}^{(0)} \otimes P_{gq}^{(0)} + 2P_{gg}^{(0)} \otimes P_{gg}^{(0)} - 5P_{gg}^{(0)}\beta_0 + 3\beta_0^2 \mathbb{1}) \otimes f_{gg}^{(0)}. \tag{23}$$

In Eqs. (16)–(23) the ⊗ products have to be understood as standard convolutions and a sum over all active quarks and antiquarks is implied as well. The coefficients of the QCD β function are given by

$$\beta_0 = \frac{1}{16\pi^2}\left(11 - \frac{2}{3}n_f\right), \qquad \beta_1 = \frac{1}{(16\pi^2)^2}\left(102 - \frac{38}{3}n_f\right). \tag{24}$$

The splitting functions $P_{ij}^{(l)}$ can be taken e.g. from Refs. [28,29]. At leading order they read

$$(16\pi^2)P_{qq}^{(0)}(x) = \frac{4}{3}\left(\frac{4}{1-x} - 2 - 2x + 3\delta(1-x)\right), \tag{25}$$

$$(16\pi^2)P_{qg}^{(0)}(x) = 2n_f(1 - 2x + 2x^2), \tag{26}$$

$$(16\pi^2)P_{gq}^{(0)}(x) = \frac{4}{3}\left(\frac{4}{x} - 4 + 2x\right), \tag{27}$$

$$(16\pi^2)P_{gg}^{(0)}(x) = 3\left(\frac{4}{1-x} + \frac{4}{x} - 8 + 4x - 4x^2 + \frac{11}{3}\delta(1-x)\right) - \frac{2}{3}n_f\delta(1-x), \tag{28}$$

where the factor $(16\pi^2)$ accounts for the normalization used in Eqs. (16)–(23). In general, we have $P_{ij}^{(l)}$(this article) $= (16\pi^2)^{-(l+1)} P_{ij}^{(l)}$(Refs. [28,29]). Please also note the explicit factor of $(2n_f)^{-1}$ in Eqs. (17)–(23), which is due to the definition of $P_{qg}^{(0)}$ in Eq. (26) and $P_{qg}^{(1)}$ in Ref. [29]. Simple fully analytic expressions for $f_{q\bar{q}}^{(11)}$, $f_{gq}^{(11)}$ and $f_{gg}^{(11)}$ are long known [9] and precise fits for all scaling functions $f_{ij}^{(21)}$, $f_{ij}^{(22)}$ in Eqs. (18)–(23), typically to per mille accuracy, are presented in the appendix in Eqs. (A1)–(A6) and Tables V, VI, and VII. Finally, the complete scale dependence for $f_{ij}(\rho, M, R)$ in Eq. (1) with $\mu_r \neq \mu_f$ is easily obtained as

$$f_{ij}(\rho, M, R) = f_{ij}(\rho, M, 1) + 4\pi\alpha_s\{2\beta_0 L_R f_{ij}^{(0)}\} + (4\pi\alpha_s)^2\{3\beta_0 L_R f_{ij}^{(10)} + 2\beta_1 L_R f_{ij}^{(0)} + 3\beta_0 L_R L_M f_{ij}^{(11)} + 3\beta_0^2 L_R^2 f_{ij}^{(0)}\}, \tag{29}$$

$$f_{gq}(\rho, M, R) = f_{gq}(\rho, M, 1) + (4\pi\alpha_s)^2\{3\beta_0 L_R f_{gq}^{(10)} + 3\beta_0 L_M f_{gq}^{(11)}\}, \tag{30}$$

where $L_R = \ln(\mu_r^2/\mu_f^2)$ and $ij = \{q\bar{q}, gg\}$ in Eq. (29).

III. PHENOMENOLOGICAL APPLICATIONS

We are now in the position to address the phenomenological consequences. The approximate NNLO prediction which includes exact dependence on all scales is based on Eqs. (12)–(14), (18)–(23), (29), and (30). If not otherwise stated, the top-quark mass is the pole mass at $m_t = 173$ GeV.

Let us start with the scale dependence of the NNLO cross section as shown in Fig. 1. Our study of the theoretical uncertainty allows us to assess the effect of independent variations of the renormalization and factorization scale μ_r and μ_f in the scaling functions for the hard partonic scattering process in Eq. (1). In doing so, one should keep in mind, however, that all currently available PDF sets from global fits always fix $\mu_r = \mu_f$. We define the theory uncertainty arising from the independent variation of μ_r and μ_f in the standard range $\mu_r, \mu_f \in [m_t/2, 2m_t]$ as

$$\min\sigma(\mu_r, \mu_f) \leq \sigma(m_t) \leq \max\sigma(\mu_r, \mu_f). \tag{31}$$

The contour lines of the total cross section for the LHC and Tevatron arising from this procedure are shown in Fig. 1. The standard range $\mu_r, \mu_f \in [m_t/2, 2m_t]$ corresponds to the region displayed in Fig. 1 because of $\log_{10}(2) \approx 0.3$. We have normalized all results to the value at $\mu_r = \mu_f = m_t$ and the variation with fixed scales $\mu_r = \mu_f$ proceeds along the diagonal from the lower left to upper right in the plots. For Tevatron in Fig. 1(b) we see that the gradient in the complete (μ_r, μ_f) plane is almost parallel to this diagonal, and thus the uncertainty according to Eq. (31) remains $-5\% \leq \Delta\sigma \leq +3\%$ in very good agreement with previous results [3,4]. At LHC in Fig. 1(a) the maximal deviations in the (μ_r, μ_f) plane are -3% located at $(2m_t, 2m_t)$ and $+1\%$ at roughly $(m_t/2, 2m_t)$, so that the uncertainty range (31) becomes slightly larger, $-3\% \leq \Delta\sigma \leq +1\%$ compared to what has been derived before with a fixed scale ratio $\mu_r = \mu_f$. Very similar numbers for both colliders are obtained with the PDF set CTEQ6.6 [7]. Also recall that we include the gq channel through two loops. Thanks to Eqs. (18)–(23) we control the exact scale dependence also for all contributions proportional to the parton luminosity L_{gq}. We conclude from Fig. 1 that the

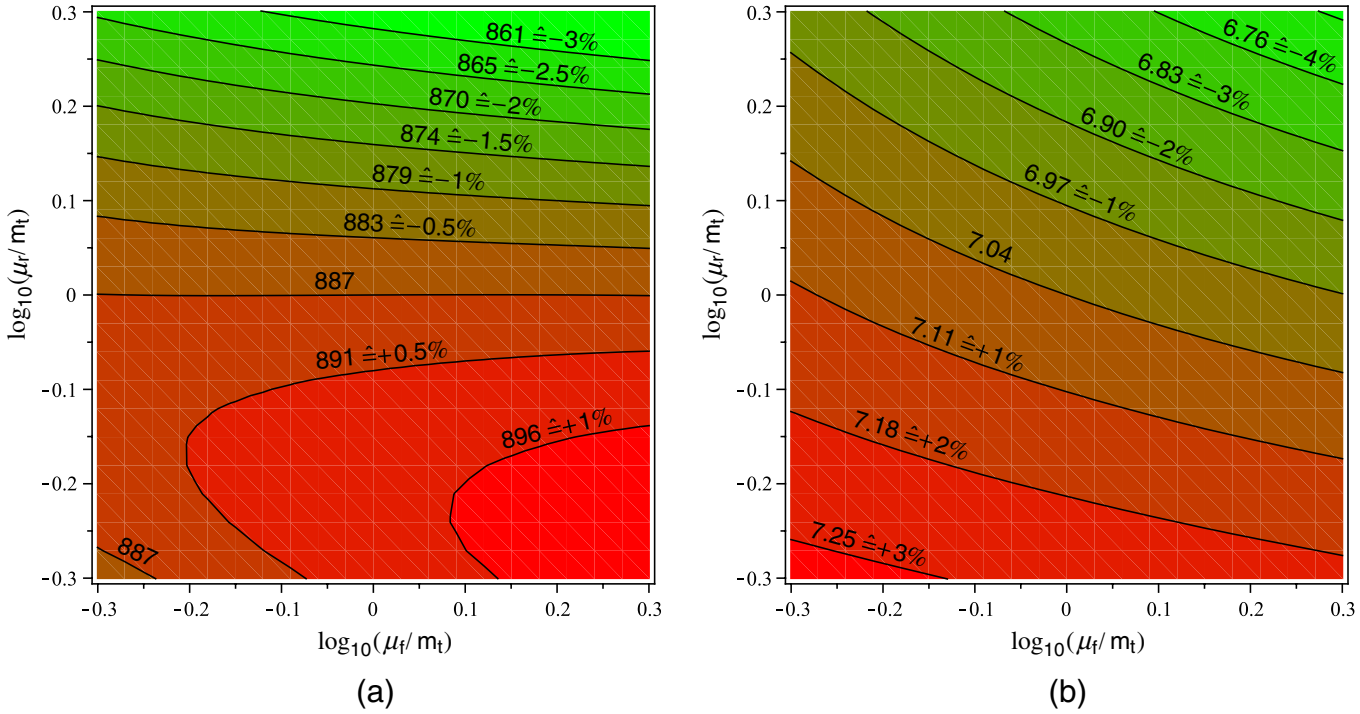

FIG. 1 (color online). The contour lines of the total hadronic cross section from the independent variation of renormalization and factorization scale μ_r and μ_f for LHC with $\sqrt{S} = 14$ TeV (left) and Tevatron with $\sqrt{S} = 1.96$ TeV (right) with MSTW 2008 [14]. The cross sections are normalized to the values at $\mu_r = \mu_f = m_t$ and the range corresponds to $\mu_r, \mu_f \in [m_t/2, 2m_t]$.

theoretical uncertainty due to μ_r and μ_f variation is well estimated by the case of identical scales $\mu_r = \mu_f$.

In order to quantify the PDF uncertainty we apply the standard definition

$$\Delta\sigma = \frac{1}{2}\sqrt{\sum_{k=1,n_{\mathrm{PDF}}} (\sigma_{k+} - \sigma_{k-})^2}, \tag{32}$$

which determines $\Delta\sigma$ from the variations $\sigma_{k\pm}$ of the cross section with respect to the k parameters of the PDF fit. Typically the PDF error is added linearly to the theory uncertainty obtained from the scale variation. This is the commonly adopted choice and we employ the PDF sets CTEQ6.6 [7] and MSTW 2008 [14]. The latter set gives two uncertainties at different confidence levels (C.L.), one at 68% C.L. and the second at 90% C.L. Throughout this study we use 68% C.L. only. Moreover in the chosen interval $\mu \in [m_t/2, 2m_t]$ for a given $\mu = \mu_r = \mu_f$ the error $\Delta\sigma(\mu)$ in Eq. (32) has only a very weak scale dependence. That is to say we find to good accuracy $\Delta\sigma(\mu = m_t/2) \simeq \Delta\sigma(\mu = m_t) \simeq \Delta\sigma(\mu = 2m_t)$ so that a determination of $\Delta\sigma$ at the central scale $\mu = m_t$ should suffice for all practical purposes.

In Fig. 2 we show the mass dependence of the total cross section, comparing the NLO and our approximate NNLO prediction. The band summarizes the total theoretical uncertainty from the linear combination of the scale uncertainty for the case $\mu_r = \mu_f$ and the PDF uncertainty Eq. (32). We display the LHC and Tevatron predictions using the MSTW 2008 PDF set [14]. The improvement of the NNLO prediction is manifest for both colliders.

Next, we discuss the sources of remaining systematical uncertainties. Undoubtedly, a complete calculation of the complete NNLO QCD corrections to hadronic top-quark pair production would be highly desirable (see Refs. [30–37] for progress in this direction). This lacking, the main systematic uncertainty of our approximate NNLO result are the subleading terms in the scaling function $f_{ij}^{(20)}$. They might become accessible by extending the approach of Refs. [26,27] or else could be modeled through power suppressed terms in Mellin space (see e.g. the scheme $A = 2$ in Ref. [38]). By including the leading term for $f_{gq}^{(20)}$ we have taken a first step in this direction and we have found numerically small effects only. In order to quantify our systematical uncertainty, we adopt the following prescription: We compute the ratio $\sigma_{\mathrm{NLL+Coul}}/\sigma_{\mathrm{exact}}$ at one loop, where $\sigma_{\mathrm{NLL+Coul}}$ only contains the Sudakov logarithms and the Coulomb terms in $f_{q\bar{q}}^{(10)}$ and $f_{gg}^{(10)}$, i.e. the content of the square brackets in Eqs. (7) and (9). This checks how well the exact hadronic cross section in Eq. (1) is approximated, if only the threshold approximation enters in the convolution with the parton luminosities. Typically we find $\sigma_{\mathrm{NLL+Coul}}/\sigma_{\mathrm{exact}} \gtrsim 0.7$ (0.9) for the LHC (Tevatron). If translated to the genuine two-loop contribution (see e.g. Table I below), then a systematic uncertainty of $\mathcal{O}(30\%)$ implies a cross section uncertainty of $\Delta\sigma \simeq \mathcal{O}(15)$ pb at

$\mu_r = \mu_f$.

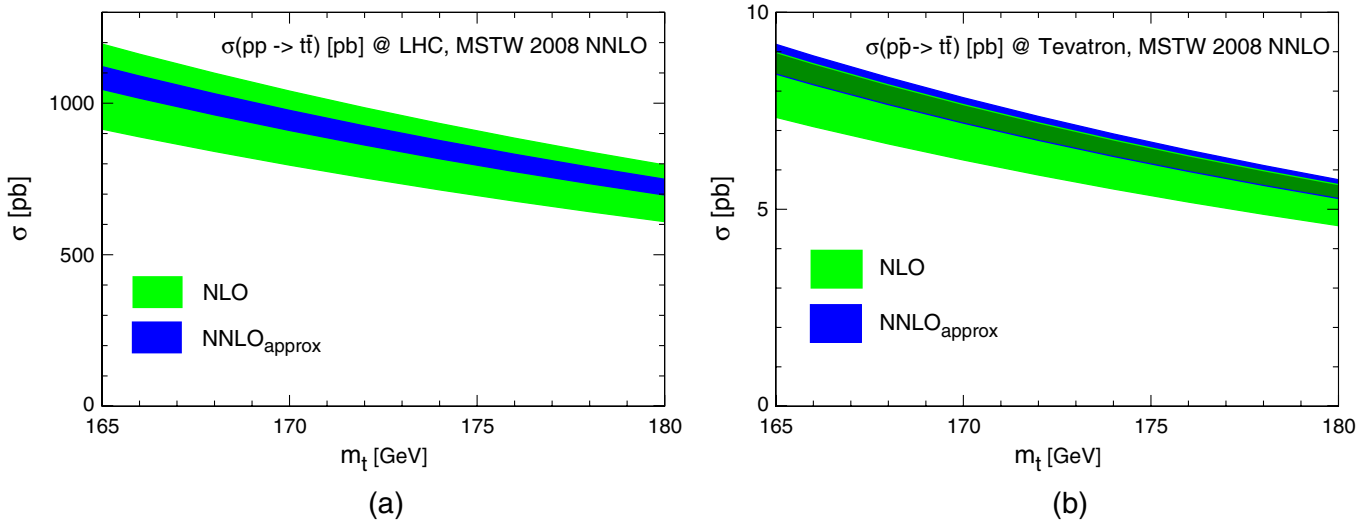

FIG. 2 (color online). The mass dependence of the total cross section at NLO (green) and approximate NNLO (blue) order for LHC at $\sqrt{S} = 14$ TeV (left) and Tevatron at $\sqrt{S} = 1.96$ TeV (right) and the PDF set MSTW 2008 [14]. The bands denote the theoretical uncertainty from scale variation keeping $\mu_r = \mu_f$ and the PDF uncertainty in the range $[m_t/2, 2m_t]$. In (b) for the Tevatron the NLO and approximate NNLO bands overlap only partially giving rise to the corresponding medium band (dark green).

LHC and of $\Delta\sigma \simeq \mathcal{O}(0.2)$ pb at Tevatron. These numbers are corroborated by other observations, like the generally small impact of the gq channel which is entirely subleading.

How does this affect the previous discussion of the scale dependence? Let us define a systematic uncertainty Δ_{sys} obtained from a variation of the scaling functions $f_{ij}^{(20)}$ in Eqs. (12)–(14) by $\pm 30\%$. All other scaling functions are known exactly anyway. The result for our NNLO cross section (always normalized to the value at $\mu = m_t$ and $\Delta_{\text{sys}} = 0$) is shown in Fig. 3 for $\mu = \mu_r = \mu_f$ and the MSTW 2008 PDF set [14]. It is obvious that the predictions are very stable within the standard range $\mu \in [m_t/2, 2m_t]$ for all cases, i.e. $\Delta_{\text{sys}} = 0$ and $\sigma \pm \Delta_{\text{sys}}$. For the case $\Delta_{\text{sys}} = 0$ we find a variation of $-3\% \leq \Delta\sigma \leq +0.5\%$ for LHC and $-5\% \leq \Delta\sigma \leq +3\%$ for Tevatron (compatible with Fig. 1) and similar numbers for the other two cases, $\sigma \pm \Delta_{\text{sys}}$.

TABLE I. The LO, NLO and approximate NNLO prediction for the total cross section at LHC ($\sqrt{S} = 14$ TeV) and Tevatron ($\sqrt{S} = 1.96$ TeV) using $m_t = 171$ GeV, the PDF set CTEQ6.6 [7] and $\mu_r = \mu_f = m_t$. For comparison we also give the previous numbers of Refs. [3,4].

	LHC	Tevatron
σ_{LO} [pb]	583.7	5.820
σ_{NLO} [pb]	877.4	7.229
σ_{NNLO} [pb] (this work)	923.0	7.814
σ_{NNLO} [pb] (Refs. [3,4])	920.5	7.810

In the present analysis, we have also neglected the effect of the new parton channels qq, $\bar{q}\,\bar{q}$ and $q_i\bar{q}_j$ (for unlike flavors $i \neq j$), which come in through real emission at NNLO only. Important insight can be gained here from the recent calculation [39,40] of the radiative corrections for $t\bar{t}$ + 1-jet production at NLO, because they represent a significant part of the complete NNLO corrections for inclusive top-quark pair production. At NLO $t\bar{t}$ + 1-jet production contains the one-loop one-parton real emissions as well as the double real emission processes, and the latter also include the above mentioned new channels. It was found that the radiative corrections at the scale $\mu_r = \mu_f = m_t$ are rather small. Depending on the kinematical cuts (e.g. on the transverse momentum of the jet) they amount to $\mathcal{O}(20)$ pb at LHC and to $\mathcal{O}(0.2)$ pb at Tevatron (see Ref. [40]). This provides further evidence that the hard corrections to the inclusive top-quark pair production at NNLO are indeed not large and it supports the estimate of our systematical uncertainty.

To summarize, our approximate NNLO prediction leaves us with a rather small residual theoretical uncertainty based on the scale variation. It is also worth stressing that the numerical impact of our theory improvements in Eqs. (12)–(14) and (18)–(23) is rather small, which again nicely illustrates the stability of the approximate NNLO predictions. In Table I we compare with our previous numbers [3,4] for the CTEQ6.6 [7] set at $m_t = 171$ GeV and $\mu_r = \mu_f = m_t$. At Tevatron, we find no changes, as the cross section is entirely dominated by the $q\bar{q}$ channel at parton kinematics close to threshold. At LHC, there is a small net change of 2.5 pb in the prediction. Here, the effect of the improved NLO matching [in particular, the

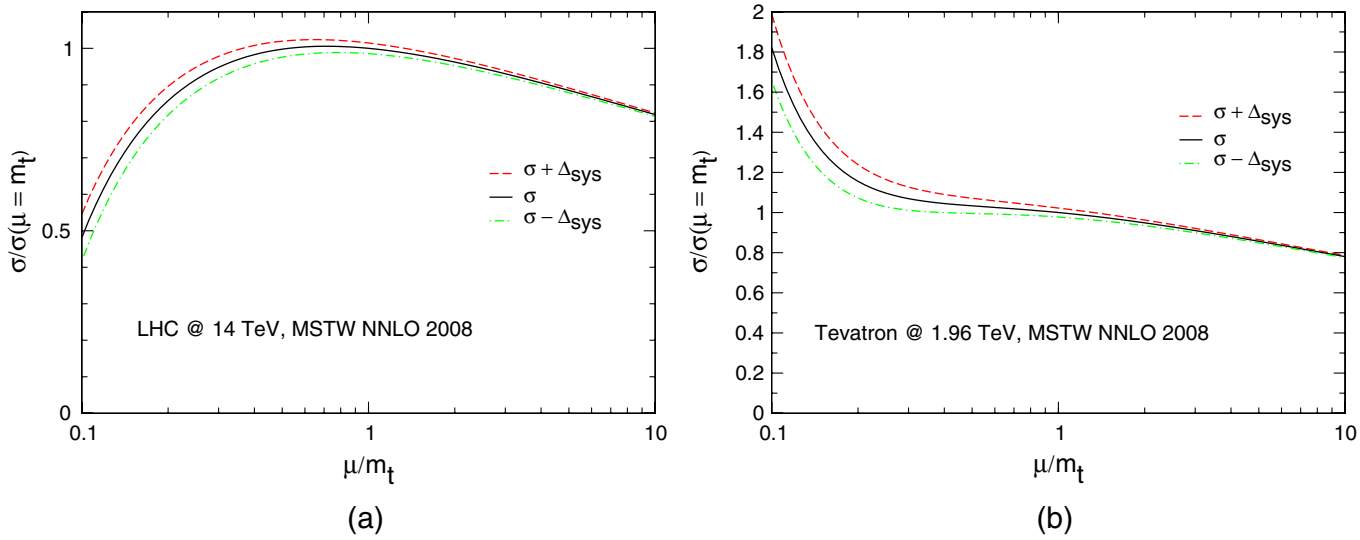

FIG. 3 (color online). The scale dependence of the approximate NNLO cross section $\sigma_{\rm NNLO}$ for the choice $\mu = \mu_r = \mu_f$ using the MSTW 2008 PDF set [14] at LHC with $\sqrt{S} = 14$ TeV (left) and Tevatron with $\sqrt{S} = 1.96$ TeV (right). $\Delta_{\rm sys}$ denotes the estimated systematic uncertainty of our threshold approximation at NNLO and all results are normalized to the value of $\sigma(\mu = m_t)$.

$\ln^2\beta$ term in Eq. (14) depending on the constant a_0^{gg} in Eq. (11)] and the leading two-loop term $f_{gq}^{(20)}$ in Eq. (13) in the gq channel partially compensate. The numerical impact of the exact color decomposition at NLO [affecting the $\ln\beta$ term in Eq. (14)] is completely negligible.

As a central result of the current studies we quote our approximate NNLO prediction at LHC ($\sqrt{S} = 14$ TeV) and Tevatron ($\sqrt{S} = 1.96$ TeV) for a pole mass of $m_t = 173$ GeV. For the MSTW 2008 set [14] we have

$$\sigma_{\rm LHC} = 887\ {\rm pb}\ {}^{+9}_{-33}\ {\rm pb\ (scale)}\ {}^{+15}_{-15}\ {\rm pb\ (MSTW\ 2008)}, \tag{33}$$

$$\sigma_{\rm Tev} = 7.04\ {\rm pb}\ {}^{+0.24}_{-0.36}\ {\rm pb\ (scale)}\ {}^{+0.14}_{-0.14}\ {\rm pb\ (MSTW\ 2008)}, \tag{34}$$

and for CTEQ6.6 [7],

$$\sigma_{\rm LHC} = 874\ {\rm pb}\ {}^{+9}_{-33}\ {\rm pb\ (scale)}\ {}^{+28}_{-28}\ {\rm pb\ (CTEQ6.6)}, \tag{35}$$

$$\sigma_{\rm Tev} = 7.34\ {\rm pb}\ {}^{+0.24}_{-0.38}\ {\rm pb\ (scale)}\ {}^{+0.41}_{-0.41}\ {\rm pb\ (CTEQ6.6)}. \tag{36}$$

Please note that the MSTW 2008 set [14] is based on a global analysis to NNLO in QCD while CTEQ6.6 [7] performs a fit to NLO only. Therefore, the two PDF sets return slightly different default values for the coupling constant α_s. While the LHC predictions of both sets are largely in agreement for these choices of α_s, the difference in the Tevatron predictions can be attributed to differences in the parametrization of the light quark PDFs at large x. In addition, there is a systematical uncertainty in Eqs. (33)–(36) estimated to be $\mathcal{O}(2\%)$ due to unknown NNLO contributions, i.e. the exact expression for $f_{ij}^{(20)}$ in Eqs. (12)–(14). One could of course argue that the accuracy of a given PDF set should match the accuracy of the theoretical prediction of the partonic cross section. However, we would like to disentangle the shift originating from corrections to the hard parton scattering (which is the main subject of our paper) from PDF effects. Therefore we always use the same order in perturbation theory as far as the chosen PDFs are concerned (cf. Table I and also Appendix B of Ref. [3]).

For applications, the mass dependence of the hadronic cross section (1) is conveniently parametrized by the following simple fit formula:

$$\sigma(m_t, \mu) = a + bx + cx^2 + dx^3 + ex^4 + fx^5 + gx^6, \tag{37}$$

with $\mu = \mu_r = \mu_f$, $x = (m_t/{\rm GeV} - 173)$ and the scale choices $\mu = m_t, 2m_t, m_t/2$. For the cross section at LHC ($\sqrt{S} = 14$ TeV and $\sqrt{S} = 10$ TeV) and Tevatron ($\sqrt{S} = 1.96$ TeV) all fit coefficients are listed in Tables III and IV,

TABLE II. The LO, NLO and approximate NNLO results for the top-quark mass in the $\overline{\rm MS}$ scheme ($\bar{m}$) and the pole mass scheme (m_t) for the measured cross section of $\sigma = 8.18$ pb at Tevatron [8]. The uncertainties in the table reflect the quoted experimental uncertainties.

	$\bar{m}$ [GeV]	m_t [GeV]
LO	$159.2^{+3.5}_{-3.4}$	$159.2^{+3.5}_{-3.4}$
NLO	$159.8^{+3.3}_{-3.3}$	$165.8^{+3.5}_{-3.5}$
NNLO	$160.0^{+3.3}_{-3.2}$	$168.2^{+3.6}_{-3.5}$

TABLE III. Fit coefficients to Eq. (37) for $\sigma(\mu = m_t, 2m_t, m_t/2)$ and $\sigma(\mu = m_t) \pm \Delta\sigma$ for the PDF set CTEQ6.6 [7] and the colliders LHC and Tevatron.

	a [pb]	b [pb]	c [pb]	d [pb]	e [pb]	f [pb]	g [pb]
LHC $\sqrt{s} = 14$ TeV, CTEQ6.6							
$\sigma(\mu = m_t)$	$8.744\,28 \times 10^{2}$	$-2.351\,92 \times 10^{1}$	$3.740\,83 \times 10^{-1}$	$-4.624\,18 \times 10^{-3}$	$4.993\,29 \times 10^{-5}$	$-4.554\,63 \times 10^{-7}$	$2.370\,50 \times 10^{-9}$
$\sigma(\mu = m_t/2)$	$8.725\,17 \times 10^{2}$	$-2.342\,60 \times 10^{1}$	$3.721\,03 \times 10^{-1}$	$-4.595\,25 \times 10^{-3}$	$4.957\,90 \times 10^{-5}$	$-4.517\,13 \times 10^{-7}$	$2.347\,71 \times 10^{-9}$
$\sigma(\mu = 2m_t)$	$8.411\,76 \times 10^{2}$	$-2.264\,14 \times 10^{1}$	$3.603\,29 \times 10^{-1}$	$-4.456\,24 \times 10^{-3}$	$4.814\,68 \times 10^{-5}$	$-4.395\,15 \times 10^{-7}$	$2.289\,15 \times 10^{-9}$
$\sigma(\mu = m_t) + \Delta\sigma$	$9.023\,78 \times 10^{2}$	$-2.409\,42 \times 10^{1}$	$3.818\,62 \times 10^{-1}$	$-4.718\,06 \times 10^{-3}$	$5.105\,68 \times 10^{-5}$	$-4.672\,81 \times 10^{-7}$	$2.438\,20 \times 10^{-9}$
$\sigma(\mu = m_t) - \Delta\sigma$	$8.464\,79 \times 10^{2}$	$-2.294\,41 \times 10^{1}$	$3.662\,98 \times 10^{-1}$	$-4.530\,09 \times 10^{-3}$	$4.881\,09 \times 10^{-5}$	$-4.437\,54 \times 10^{-7}$	$2.303\,62 \times 10^{-9}$
LHC $\sqrt{s} = 10$ TeV, CTEQ6.6							
$\sigma(\mu = m_t)$	$3.968\,77 \times 10^{2}$	$-1.120\,77 \times 10^{1}$	$1.853\,52 \times 10^{-1}$	$-2.366\,59 \times 10^{-3}$	$2.628\,00 \times 10^{-5}$	$-2.448\,41 \times 10^{-7}$	$1.289\,59 \times 10^{-9}$
$\sigma(\mu = m_t/2)$	$3.971\,24 \times 10^{2}$	$-1.118\,89 \times 10^{1}$	$1.847\,06 \times 10^{-1}$	$-2.355\,01 \times 10^{-3}$	$2.611\,83 \times 10^{-5}$	$-2.429\,89 \times 10^{-7}$	$1.278\,05 \times 10^{-9}$
$\sigma(\mu = 2m_t)$	$3.798\,52 \times 10^{2}$	$-1.073\,58 \times 10^{1}$	$1.776\,67 \times 10^{-1}$	$-2.269\,77 \times 10^{-3}$	$2.522\,23 \times 10^{-5}$	$-2.352\,20 \times 10^{-7}$	$1.240\,16 \times 10^{-9}$
$\sigma(\mu = m_t) + \Delta\sigma$	$4.151\,25 \times 10^{2}$	$-1.159\,47 \times 10^{1}$	$1.902\,85 \times 10^{-1}$	$-2.417\,72 \times 10^{-3}$	$2.678\,43 \times 10^{-5}$	$-2.494\,80 \times 10^{-7}$	$1.314\,88 \times 10^{-9}$
$\sigma(\mu = m_t) - \Delta\sigma$	$3.786\,28 \times 10^{2}$	$-1.082\,07 \times 10^{1}$	$1.804\,16 \times 10^{-1}$	$-2.315\,32 \times 10^{-3}$	$2.577\,69 \times 10^{-5}$	$-2.403\,23 \times 10^{-7}$	$1.265\,69 \times 10^{-9}$
Tevatron $\sqrt{s} = 1.96$ TeV, CTEQ6.6							
$\sigma(\mu = m_t)$	$7.343\,17 \times 10^{0}$	$-2.274\,86 \times 10^{-1}$	$3.940\,86 \times 10^{-3}$	$-5.223\,02 \times 10^{-5}$	$6.094\,97 \times 10^{-7}$	$-5.994\,14 \times 10^{-9}$	$3.279\,25 \times 10^{-11}$
$\sigma(\mu = m_t/2)$	$7.583\,12 \times 10^{0}$	$-2.345\,71 \times 10^{-1}$	$4.058\,22 \times 10^{-3}$	$-5.370\,18 \times 10^{-5}$	$6.254\,08 \times 10^{-7}$	$-6.139\,01 \times 10^{-9}$	$3.354\,67 \times 10^{-11}$
$\sigma(\mu = 2m_t)$	$6.963\,03 \times 10^{0}$	$-2.157\,48 \times 10^{-1}$	$3.731\,28 \times 10^{-3}$	$-4.930\,12 \times 10^{-5}$	$5.732\,18 \times 10^{-7}$	$-5.620\,92 \times 10^{-9}$	$3.070\,38 \times 10^{-11}$
$\sigma(\mu = m_t) + \Delta\sigma$	$7.758\,54 \times 10^{0}$	$-2.422\,54 \times 10^{-1}$	$4.236\,65 \times 10^{-3}$	$-5.659\,55 \times 10^{-5}$	$6.632\,96 \times 10^{-7}$	$-6.529\,35 \times 10^{-9}$	$3.570\,62 \times 10^{-11}$
$\sigma(\mu = m_t) - \Delta\sigma$	$6.927\,80 \times 10^{0}$	$-2.127\,18 \times 10^{-1}$	$3.645\,06 \times 10^{-3}$	$-4.786\,28 \times 10^{-5}$	$5.556\,79 \times 10^{-7}$	$-5.460\,23 \times 10^{-9}$	$2.990\,03 \times 10^{-11}$

where we have used the PDF sets CTEQ6.6 [7] and MSTW 2008 [14]. In the mass range 150 GeV $\leq m_t \leq$ 220 GeV, the accuracy of the fit is always better than 2.5‰.

Let us briefly mention also other types of radiative corrections, which have not been considered here, e.g. in Eqs. (33)–(37). Within QCD these are bound state effects for the $t\bar{t}$ pair near threshold [18,19]. They affect the total cross section at LHC of the order $\mathcal{O}(10)$ pb and, even more so, differential distributions in the invariant mass of the top-quark pair. At Tevatron, due to the dominance of the $q\bar{q}$ channel in the color-octet configuration, they are negligible though. Precision analyses at the percent level naturally need to consider also the electroweak radiative corrections at NLO [20–22]. Depending on the Higgs mass they cause a decrease relative to the LO cross section between $\mathcal{O}(2\%)$ for a light Higgs ($m_h = 120$ GeV) and $\mathcal{O}(2.5\%)$ for a heavy Higgs ($m_h = 1000$ GeV) at the LHC. This amounts to a negative contribution $\Delta\sigma_{\mathrm{EW}} \simeq \mathcal{O}(10\text{–}15)$ pb. At the Tevatron, the electroweak radiative corrections are almost zero for a light Higgs ($m_h = 120$ GeV) and give a negative contribution of order $\mathcal{O}(1\%)$, i.e. $\Delta\sigma_{\mathrm{EW}} \simeq \mathcal{O}(0.05)$ pb for a heavy Higgs ($m_h = 1000$ GeV).

TABLE IV. Same as Table III for the PDF set MSTW2008 [14] at NNLO. The PDF uncertainty $\Delta\sigma$ has been obtained with the 68% confidence level set.

	a [pb]	b [pb]	c [pb]	d [pb]	e [pb]	f [pb]	g [pb]
LHC $\sqrt{s} = 14$ TeV, MSTW 2008 NNLO							
$\sigma(\mu = m_t)$	$8.874\,96 \times 10^{2}$	$-2.383\,44 \times 10^{1}$	$3.782\,24 \times 10^{-1}$	$-4.663\,07 \times 10^{-3}$	$5.021\,55 \times 10^{-5}$	$-4.569\,10 \times 10^{-7}$	$2.373\,74 \times 10^{-9}$
$\sigma(\mu = m_t/2)$	$8.855\,30 \times 10^{2}$	$-2.373\,87 \times 10^{1}$	$3.762\,03 \times 10^{-1}$	$-4.633\,31 \times 10^{-3}$	$4.984\,11 \times 10^{-5}$	$-4.529\,80 \times 10^{-7}$	$2.351\,37 \times 10^{-9}$
$\sigma(\mu = 2m_t)$	$8.540\,52 \times 10^{2}$	$-2.295\,66 \times 10^{1}$	$3.645\,47 \times 10^{-1}$	$-4.496\,61 \times 10^{-3}$	$4.845\,39 \times 10^{-5}$	$-4.415\,74 \times 10^{-7}$	$2.299\,07 \times 10^{-9}$
$\sigma(\mu = m_t) + \Delta\sigma$	$9.029\,02 \times 10^{2}$	$-2.419\,07 \times 10^{1}$	$3.831\,90 \times 10^{-1}$	$-4.718\,08 \times 10^{-3}$	$5.076\,42 \times 10^{-5}$	$-4.618\,04 \times 10^{-7}$	$2.399\,89 \times 10^{-9}$
$\sigma(\mu = m_t) - \Delta\sigma$	$8.720\,90 \times 10^{2}$	$-2.347\,83 \times 10^{1}$	$3.732\,57 \times 10^{-1}$	$-4.607\,76 \times 10^{-3}$	$4.966\,61 \times 10^{-5}$	$-4.522\,97 \times 10^{-7}$	$2.351\,68 \times 10^{-9}$
LHC $\sqrt{s} = 10$ TeV, MSTW 2008 NNLO							
$\sigma(\mu = m_t)$	$4.032\,19 \times 10^{2}$	$-1.139\,04 \times 10^{1}$	$1.881\,77 \times 10^{-1}$	$-2.398\,35 \times 10^{-3}$	$2.658\,11 \times 10^{-5}$	$-2.473\,37 \times 10^{-7}$	$1.302\,17 \times 10^{-9}$
$\sigma(\mu = m_t/2)$	$4.034\,39 \times 10^{2}$	$-1.136\,95 \times 10^{1}$	$1.874\,88 \times 10^{-1}$	$-2.386\,25 \times 10^{-3}$	$2.640\,67 \times 10^{-5}$	$-2.451\,91 \times 10^{-7}$	$1.288\,31 \times 10^{-9}$
$\sigma(\mu = 2m_t)$	$3.860\,12 \times 10^{2}$	$-1.091\,54 \times 10^{1}$	$1.804\,86 \times 10^{-1}$	$-2.301\,94 \times 10^{-3}$	$2.552\,75 \times 10^{-5}$	$-2.377\,10 \times 10^{-7}$	$1.252\,72 \times 10^{-9}$
$\sigma(\mu = m_t) + \Delta\sigma$	$4.119\,12 \times 10^{2}$	$-1.160\,47 \times 10^{1}$	$1.912\,87 \times 10^{-1}$	$-2.433\,44 \times 10^{-3}$	$2.692\,97 \times 10^{-5}$	$-2.503\,69 \times 10^{-7}$	$1.317\,93 \times 10^{-9}$
$\sigma(\mu = m_t) - \Delta\sigma$	$3.945\,26 \times 10^{2}$	$-1.117\,61 \times 10^{1}$	$1.850\,66 \times 10^{-1}$	$-2.363\,10 \times 10^{-3}$	$2.623\,15 \times 10^{-5}$	$-2.444\,19 \times 10^{-7}$	$1.288\,19 \times 10^{-9}$
Tevatron $\sqrt{s} = 1.96$ TeV, MSTW 2008 NNLO							
$\sigma(\mu = m_t)$	$7.042\,17 \times 10^{0}$	$-2.188\,00 \times 10^{-1}$	$3.803\,66 \times 10^{-3}$	$-5.067\,95 \times 10^{-5}$	$5.963\,08 \times 10^{-7}$	$-5.921\,50 \times 10^{-9}$	$3.263\,69 \times 10^{-11}$
$\sigma(\mu = m_t/2)$	$7.277\,46 \times 10^{0}$	$-2.257\,94 \times 10^{-1}$	$3.920\,60 \times 10^{-3}$	$-5.218\,16 \times 10^{-5}$	$6.126\,61 \times 10^{-7}$	$-6.057\,62 \times 10^{-9}$	$3.323\,60 \times 10^{-11}$
$\sigma(\mu = 2m_t)$	$6.679\,70 \times 10^{0}$	$-2.075\,17 \times 10^{-1}$	$3.600\,70 \times 10^{-3}$	$-4.782\,94 \times 10^{-5}$	$5.601\,41 \times 10^{-7}$	$-5.526\,80 \times 10^{-9}$	$3.028\,83 \times 10^{-11}$
$\sigma(\mu = m_t) + \Delta\sigma$	$7.184\,07 \times 10^{0}$	$-2.224\,29 \times 10^{-1}$	$3.855\,13 \times 10^{-3}$	$-5.131\,71 \times 10^{-5}$	$6.054\,82 \times 10^{-7}$	$-6.043\,97 \times 10^{-9}$	$3.345\,49 \times 10^{-11}$
$\sigma(\mu = m_t) - \Delta\sigma$	$6.900\,28 \times 10^{0}$	$-2.151\,71 \times 10^{-1}$	$3.752\,14 \times 10^{-3}$	$-5.003\,94 \times 10^{-5}$	$5.871\,70 \times 10^{-7}$	$-5.802\,14 \times 10^{-9}$	$3.185\,53 \times 10^{-11}$

IV. THE TOP-QUARK MASS IN THE $\overline{\text{MS}}$ SCHEME

So far we have used the pole mass of the top quark as a definition of the mass parameter. However, it is well known that the concept of the pole mass has intrinsic theoretical limitations owing to the fact that the top quark is a colored object. As such it does not appear as an asymptotic state of the S matrix due to confinement. In other words the S matrix does not have a pole in the top-quark channel. The impact of different mass renormalizations has been investigated in great detail in the context of top-quark mass measurements at a future linear collider where a precision of the order of a few hundred MeV is envisaged. In particular, it has been shown that indeed the conceptual limitations of the pole mass lead to a poorly behaved perturbative series. A class of alternative mass definitions, so-called short distance masses, offer a solution to this problem, e.g. the $1S$ mass or the potential subtracted mass (see e.g. Ref. [41]).

In the following we study the impact of the conversion from the pole mass scheme to the $\overline{\text{MS}}$ scheme (see Refs. [23–25], and references therein) for the total cross section of top-quark hadroproduction. This is a novel feature and, in principle, the cross section in terms of the $\overline{\text{MS}}$ mass can be used for a direct measurement of the running mass at a high scale. This is similar to the case of b-quark production at LEP (see Refs. [42–47]). Let us first describe briefly how we translate the predictions for the total cross section from the pole mass to the $\overline{\text{MS}}$ mass scheme. The starting point is the well-known relation between the pole mass m_t and the $\overline{\text{MS}}$ mass $m(\mu_r)$ to NNLO:

$$m_t = m(\mu_r)(1 + a_s(\mu_r)d^{(1)} + a_s(\mu_r)^2 d^{(2)}), \tag{38}$$

with $a_s = \alpha_s^{(n_f=5)}/\pi$ (i.e. five active flavors) and coefficients $d^{(i)}$, which in general depend on the ratio $\mu_r^2/m(\mu_r)^2$,

$$d^{(1)} = \frac{4}{3} + L_{m(\mu_r)}, \tag{39}$$

$$\begin{aligned} d^{(2)} = {} & \frac{307}{32} + 2\zeta_2 + \frac{2}{3}\zeta_2 \ln 2 - \frac{1}{6}\zeta_3 + \frac{509}{72}L_{m(\mu_r)} \\ & + \frac{47}{24}L_{m(\mu_r)}^2 - \left(\frac{71}{144} + \frac{1}{3}\zeta_2 + \frac{13}{36}L_{m(\mu_r)} \right. \\ & \left. + \frac{1}{12}L_{m(\mu_r)}^2\right)n_f + \frac{4}{3}\sum_i \Delta(m_i/m_t). \end{aligned} \tag{40}$$

Here n_f denotes the number of light flavors and $L_{m(\mu_r)} = \ln(\mu_r^2/m(\mu_r)^2)$. The function $\Delta(m_i/m_t)$ accounts for all massive quarks m_i lighter than the top quark. For all light quarks we set $m_i = 0$ so the sum in Eq. (40) vanishes. Note also that the decoupling of the top quark is assumed to be done at the scale of the $\overline{\text{MS}}$ mass $m(\mu_r)$.

Let us start by making the mass dependence in the total cross section manifest order by order in perturbation theory. For the pole mass m_t we have through NNLO

$$\sigma = a_s^2 \sum_{i=0}^{2} a_s^i \sigma^{(i)}(m_t). \tag{41}$$

Next, we use the relation (38) above to convert from the pole mass to the $\overline{\text{MS}}$ mass $m(m)$. For simplicity we abbreviate $\bar{m} = m(m)$ and obtain

$$\begin{aligned} \sigma = a_s^2 \sum_{i=0}^{2} a_s^i \Bigg(& \sigma^{(i)}(\bar{m}) + \bar{m} \sum_{l=1}^{i} d^{(l)} \partial_m \sigma^{(i-l)}(m)|_{m=\bar{m}} \\ & + \delta_{i,2} \frac{1}{2}(\bar{m} d^{(1)})^2 \partial_m^2 \sigma^{(0)}(m)|_{m=\bar{m}} \Bigg). \end{aligned} \tag{42}$$

We note that the coefficients $d^{(i)}$ have to be evaluated for $\mu_r = \bar{m}$ (corresponding to the scale of α_s). Thus, the task in Eq. (42) amounts to determine the derivatives of the cross sections $\sigma^{(i)}$ with respect to the mass. To do so in practice we have chosen the following approach. For all coefficients $\sigma^{(i)}$ we use the ansatz of Eq. (47) to parametrize the mass dependence. More precisely we evaluate the hadronic cross section order by order in perturbation theory for a fixed renormalization and factorization scale. Then, varying the top-quark mass (in the pole mass scheme) and performing a fit similar to what has been discussed before in Eq. (37) we obtain the total cross section in the following form:

$$\sigma = a_s^2 \sum_{i=0}^{2} a_s^i \sum_{k=0}^{N} (m_t - m_0)^k c_k^{(i)}, \tag{43}$$

where $c_k^{(i)}$ denote the (order-dependent) fit coefficients. N is the order of the polynomial in m_t [$N = 6$ in Eq. (37)] and m_0 is our fixed reference mass [taken to be 173 GeV in Eq. (37)]. Since all dependence on the pole mass m_t is manifest, it is now a straightforward exercise to convert to the $\overline{\text{MS}}$ mass $\bar{m}$ and to perform the derivatives in Eq. (42),

$$\begin{aligned} \sigma = {} & a_s^2 \sum_{i=0}^{2} a_s^i \sum_{k=0}^{N} \Bigg((\bar{m} - m_0)^k c_k^{(i)} + k\bar{m}(\bar{m} - m_0)^{k-1} \\ & \times \sum_{l=1}^{i} d^{(l)} c_k^{(i-l)} + \delta_{i,2} \frac{1}{2} k(k-1) \\ & \times \bar{m}^2 (\bar{m} - m_0)^{k-2} (d^{(1)})^2 c_k^{(0)} \Bigg) \\ \overset{m_0=\bar{m}}{=} {} & a_s^2 (c_0^{(0)} + a_s\{c_0^{(1)} + \bar{m} d^{(1)} c_1^{(0)}\} + a_s^2\{c_0^{(2)} + \bar{m} d^{(1)} c_1^{(1)} \\ & + \bar{m} d^{(2)} c_1^{(0)} + \bar{m}^2 (d^{(1)})^2 c_2^{(0)}\}). \end{aligned} \tag{44}$$

If the expansion point m_0 is chosen to be the $\overline{\text{MS}}$ mass $\bar{m}$, Eq. (44) simplifies considerably and the truncation of the power series in $\bar{m}$ to first (second) order is exact at NLO (NNLO). Generally though, for applications, it is of some advantage to keep m_0 at a fixed numerical value and to rely

on the fact that our ansatz (43) with a polynomial of high enough degree N approximates all coefficients $\sigma^{(i)}$ and their first two derivatives sufficiently well. As discussed below Eq. (37), the choice $N = 6$ achieves per mille accuracy in the phenomenologically interesting range. We have also checked that the choices $m_0 = \bar{m}$ and $m_0 \neq \bar{m}$ yield the same result.

We stress again that we have fixed $\mu_r = \bar{m}$ in Eq. (44). However, it is also possible to restore the complete renormalization scale dependence using the well-known relation for the running coupling

$$a_s(\bar{m}) = a_s(\mu_r)(1 + 4\pi^2 a_s(\mu_r) L_{\bar{R}} \beta_0 + (4\pi^2)^2 a_s(\mu_r)^2 (\beta_1 L_{\bar{R}} + \beta_0^2 L_{\bar{R}}^2)), \quad (45)$$

with $L_{\bar{R}} = \ln(\mu_r^2/\bar{m}^2)$ and β_0 and β_1 given in Eq. (24). To summarize, Eq. (44) represents an explicit expression for the total cross section of top-quark hadroproduction with the top-quark mass defined in the $\overline{\text{MS}}$ scheme.

Let us illustrate the phenomenological consequences of the $\overline{\text{MS}}$ mass for predictions at Tevatron and LHC. In Fig. 4 we plot the scale dependence of the total cross section again at the various orders in perturbation theory. The value of $\bar{m} = 163$ GeV roughly corresponds to a pole mass of $m_t = 173$ GeV and we choose three (fixed) values for the factorization scale $\mu_f = \bar{m}/2$, $\bar{m}$ and $2\bar{m}$. The band to the left denotes the maximum and the minimum values of $\mu_r \in [\bar{m}/2, 2\bar{m}]$ for the three choices of μ_f according to Eq. (31); cf. the contour plot in Fig. 1 for the pole mass. We observe a great stability with respect to scale variations when including higher order perturbative corrections through NNLO. Remarkably, at Tevatron, the scale variation at NNLO is even reduced further by more than a factor of 2 compared to the result in the pole mass scheme.

Next, in Fig. 5 we show the mass dependence of the total cross section employing the $\overline{\text{MS}}$ mass definition and performing the same scale variation as above, i.e. $\mu_f = \bar{m}/2$, $\bar{m}$ and $2\bar{m}$ and $\mu_r \in [\bar{m}/2, 2\bar{m}]$. Upon adding the higher order perturbative corrections we observe as a striking feature the extremely small numerical effect of the radiative corrections. For example, for $\bar{m} = 163$ GeV at Tevatron, we find the effect of the NLO corrections to be only 1.5% and even less (0.9%) for the approximate NNLO results. Also for the LHC, we observe a much faster convergence of the perturbative expansion when using the $\overline{\text{MS}}$ mass. The NLO (approximate NNLO) corrections amount to 31% (4%) at $\bar{m} = 163$ GeV which is roughly half of the size of the corrections in the pole mass scheme. This demonstrates an extremely good stability of the perturbative series in the $\overline{\text{MS}}$ mass scheme. We can understand this behavior qualitatively by looking at the mass dependence of the scaling functions in Eqs. (4)–(9). We find e.g. $\partial_m f_{ij}^{(0)} \simeq (1 - \beta^2)/\beta$, which implies sizably enhanced contributions near partonic threshold, i.e. precisely in the region which contributes dominantly in the convolution with the parton luminosities; cf. Eq. (1). This observation is yet another argument in favor of the phenomenological importance of our approximate NNLO predictions in Eqs. (12)–(14).

A different way to address the issue of perturbative stability is the extraction of the $\overline{\text{MS}}$ mass from the total

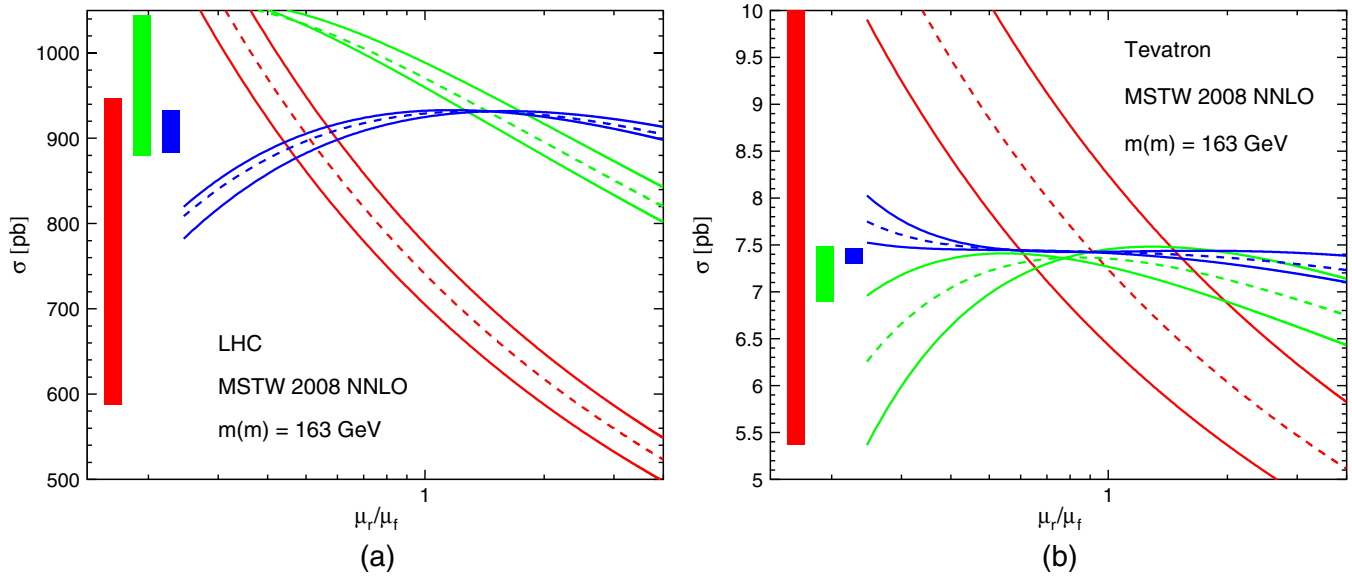

FIG. 4 (color online). The scale dependence of the total cross section with the top-quark mass in the $\overline{\text{MS}}$ scheme at $\bar{m} = 163$ GeV at LO (red), NLO (green) and approximate NNLO (blue). The dashed lines denote the $\mu_f = \bar{m}$ for the factorization scale, the solid lines the maximal deviations for $\mu_r \in [\bar{m}/2, 2\bar{m}]$ and $\mu_f = \bar{m}/2$, $\bar{m}$ and $2\bar{m}$. We use the MSTW 2008 PDF set [14] at LHC with $\sqrt{S} = 14$ TeV (left) and Tevatron with $\sqrt{S} = 1.96$ TeV (right). The vertical bars indicate the size of the scale variation in the standard range $[\bar{m}/2, 2\bar{m}]$.

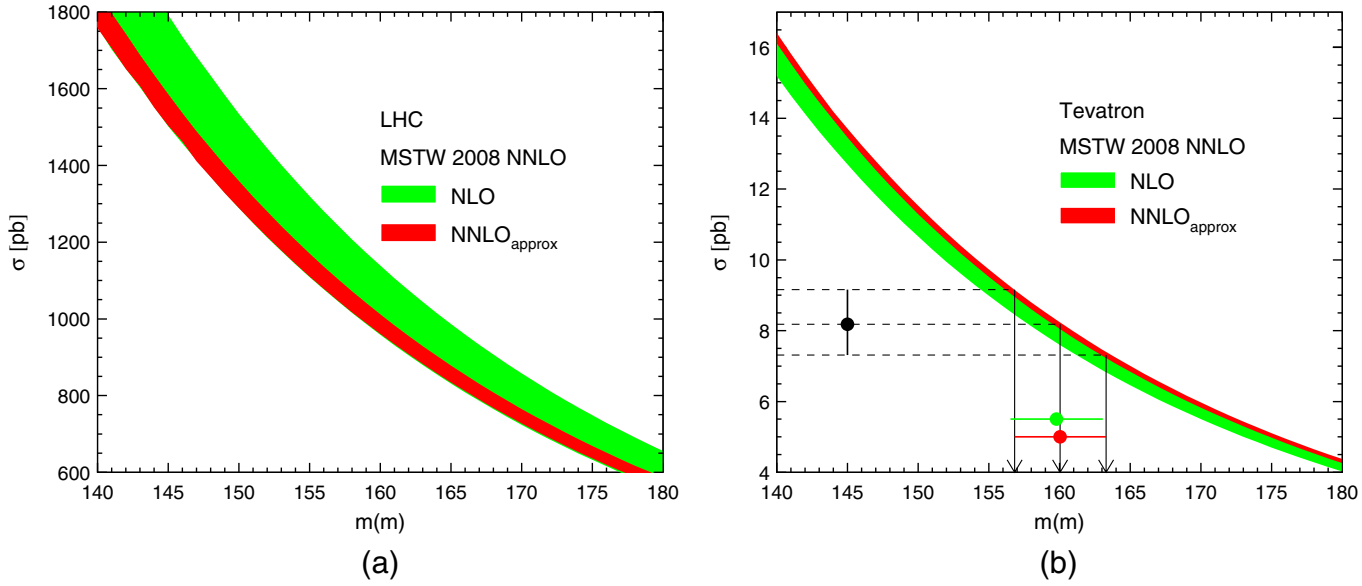

FIG. 5 (color online). The mass dependence of the total cross section for the $\overline{\text{MS}}$ mass $\bar{m}$ at NLO (green) and approximate NNLO (red) order with the scale variation in the range $\mu_r \in [\bar{m}/2, 2\bar{m}]$ and $\mu_f = \bar{m}/2$, $\bar{m}$ and $2\bar{m}$ for the MSTW 2008 PDF set [14] at LHC with $\sqrt{S} = 14$ TeV (left) and Tevatron with $\sqrt{S} = 1.96$ TeV (right). The value for the Tevatron cross section is taken from Ref. [8].

cross section as measured at Tevatron. Reference [8] quotes a value with a combined uncertainty of $\sigma = 8.18^{+0.98}_{-0.87}$ pb for a top-quark mass $m_t = 170$ GeV along with a (weak) dependence on the value of the mass, e.g. $\sigma = 7.99$ pb for the latest world average [13], $m_t = 173.1^{+1.3}_{-1.3}$ GeV. Using the measured value of $\sigma = 8.18$ pb which is consistent with the theory predictions of Refs. [3,4] (and with this work; see Table II) we extract the $\overline{\text{MS}}$ mass $\bar{m}$ order by order. As mentioned earlier we use the same NNLO PDF set of MSTW 2008 [14] independent of the order of perturbation theory and the results at LO, NLO and approximate NNLO are given in Table II. The value of $\bar{m} = 160.0^{+3.3}_{-3.2}$ GeV represents to the best of our knowledge the first direct determination of the running top-quark mass from experimental data. For comparison, we also quote the values of the pole mass m_t at the respective order extracted in the same way by directly comparing the theory prediction with the measured cross section. Alternatively, we can also convert the $\overline{\text{MS}}$ mass value back to the pole mass scheme with the help of Eq. (38). Our NNLO value for $\bar{m}$ corresponds to $m_t = 168.9^{+3.5}_{-3.4}$ GeV, which constitutes a theoretically well-defined determination of the pole mass and is also (within the experimental uncertainties) in agreement with the world average [13] of $m_t = 173.1^{+1.3}_{-1.3}$GeV. To summarize, the $\overline{\text{MS}}$ mass scheme is distinguished by the great stability in the value of the extracted top-quark mass. This feature has been studied in the past in detail for processes at a future linear collider [41] and our observation is also in agreement with recent considerations based on the renormalization group flow for heavy quark masses [48].

V. SUMMARY

In this Letter, we update and extend the predictions of Refs. [3,4] for the cross section of top-quark hadroproduction at LHC and Tevatron. We have applied some improvements in the threshold approximation for the two-loop scaling functions (12)–(14) as described in the text. We provide new and precise parametrizations in Eqs. (7)–(9) and (18)–(23) for all scaling functions that can be determined exactly. All fit functions are documented in the appendix. Moreover, we have performed the independent variation of the renormalization and the factorization scale with the help of Eqs. (29) and (30). As a novel aspect, in addition to the conventionally used pole mass we provide predictions for the total cross section employing the $\overline{\text{MS}}$ definition for the mass parameter. The central result is Eq. (44).

Our main phenomenological results are the parametrizations in Eq. (37), Tables III and IV and the cross sections in Eqs. (33)–(36) for the pole mass. The differences with respect to our previous numbers are quite small, though; see Table I. The theory uncertainty according to Eq. (31) defined by exploring the (μ_r, μ_f) plane in the standard range $\mu_r, \mu_f \in [m_t/2, 2m_t]$ does not differ significantly from the case of fixed scales $\mu_r = \mu_f$. We have also addressed the residual systematical uncertainty due to the threshold approximation and we have quantified the effect of other higher order corrections, such as electroweak or QCD bound state effects. The most interesting aspect of our phenomenological studies consists of the conversion to the $\overline{\text{MS}}$ mass scheme in Figs. 4 and 5. The cross section predictions with the $\overline{\text{MS}}$ mass definition exhibit a greatly

improved pattern of apparent convergence for the perturbative expansion and very good stability with respect to scale variations. This leads to very stable values for the extracted mass parameter $\bar{m}$ as given in Table II. In particular, we find

$$\bar{m} = 160.0^{+3.3}_{-3.2}\ \text{GeV}. \tag{46}$$

This is the first direct determination of the running top-quark mass from top-quark pair production. The corresponding value for the pole mass derived from Eq. (46) reads

$$m_t = 168.9^{+3.5}_{-3.4}\ \text{GeV}, \tag{47}$$

which is consistent with the current world average [13], $m_t = 173.1^{+1.3}_{-1.3}$ GeV. Altogether, this provides substantial support in view of the reliability of our approximate NNLO numbers. We believe that the QCD radiative corrections for top-quark pair production at hadron colliders are well under control.

ACKNOWLEDGMENTS

We would like to thank W. Bernreuther, M. Cacciari, A. Hoang and H. Kawamura for stimulating discussions and A. Mitov for his very lively contributions at LoopFest VIII and the CERN Theory Institute *TOP09*. This work is supported by the Helmholtz Gemeinschaft under Contract No. VH-NG-105 and by the Deutsche Forschungsgemeinschaft under Contract No. SFB/TR 9. P. U. acknowledges the support of the Initiative and Networking Fund of the Helmholtz Gemeinschaft, Contract No. HA-101 (''Physics at the Terascale'').

APPENDIX: USEFUL FORMULAS

$$f_{q\bar{q}}^{(21)} = \frac{1}{(16\pi^2)^2} f_{q\bar{q}}^{(0)} \left[-\frac{8192}{9}\ln^3\beta + \left(\frac{12\,928}{3} - \frac{32\,768}{9}\ln 2\right)\ln^2\beta + \left(-840.510\,65 + 70.183\,854\,\frac{1}{\beta}\right)\ln\beta - 82.246\,703\,\frac{1}{\beta} + 467.904\,02 \right] + \frac{n_f}{(16\pi^2)^2} f_{q\bar{q}}^{(0)} \left[-\frac{256}{3}\ln^2\beta + \left(\frac{2608}{9} - \frac{2816}{9}\ln 2\right)\ln\beta + 6.579\,736\,3\,\frac{1}{\beta} - 64.614\,276 \right] + h(\beta, b_i + n_f c_i) - \frac{4n_f^2}{(16\pi^2)^2} f_{q\bar{q}}^{(0)} \left[\frac{4}{3}\ln 2 - \frac{2}{3}\ln\rho - \frac{10}{9} \right], \tag{A1}$$

$$f_{q\bar{q}}^{(22)} = \frac{1}{(16\pi^2)^2} f_{q\bar{q}}^{(0)} \left[\frac{2048}{9}\ln^2\beta + \left(-\frac{7840}{9} + \frac{4096}{9}\ln 2\right)\ln\beta + 270.897\,24 \right] + \frac{n_f}{(16\pi^2)^2} f_{q\bar{q}}^{(0)} \left[\frac{320}{9}\ln\beta - \frac{596}{9} + \frac{320}{9}\ln 2 \right] + h(\beta, b_i + n_f c_i) + \frac{4n_f^2}{3(16\pi^2)^2} f_{q\bar{q}}^{(0)}, \tag{A2}$$

$$f_{gq}^{(21)} = -\frac{\pi}{(16\pi^2)^2}\beta^3 \left[\frac{770}{27}\ln^2\beta + \left(-\frac{6805}{81} + \frac{6160}{81}\ln 2\right)\ln\beta + 0.137\,077\,84\,\frac{1}{\beta} + 0.220\,688\,68 \right] - \frac{\pi n_f}{81(16\pi^2)^2}\beta^3 \left[46\ln\beta - \frac{163}{3} + 76\ln 2 \right] + h_{gq}^{(b)}(\beta, b_i + n_f c_i), \tag{A3}$$

$$f_{gq}^{(22)} = \frac{\pi}{(16\pi^2)^2}\beta^3 \left[\frac{385}{81}\ln\beta - \frac{1540}{243} + \frac{385}{81}\ln 2 \right] + h_{gq}^{(b)}(\beta, b_i + n_f c_i), \tag{A4}$$

$$f_{gg}^{(21)} = \frac{1}{(16\pi^2)^2} f_{gg}^{(0)} \left[-4608\ln^3\beta + \left(\frac{109\,920}{7} - 18\,432\ln 2\right)\ln^2\beta + \left(69.647\,185 - 248.150\,05\,\frac{1}{\beta}\right)\ln\beta + 56.867\,721\,\frac{1}{\beta} + 17.010\,070 \right] + \frac{n_f}{(16\pi^2)^2} f_{gg}^{(0)} \left[-64\ln^2\beta + \left(\frac{4048}{21} - 192\ln 2\right)\ln\beta - 3.446\,528\,5\,\frac{1}{\beta} - 37.602\,004 \right] + h(\beta, b_i + n_f c_i), \tag{A5}$$

TABLE V. Coefficients for fits of the $q\bar{q}$ scaling functions.

	$f_{q\bar{q}}^{(10)}$	$f_{q\bar{q}}^{(21)}$		$f_{q\bar{q}}^{(22)}$	
i	a_i	b_i	c_i	b_i	c_i
1	0.071 206 03	−0.153 887 65	−0.079 606 58	0.379 470 56	−0.002 241 14
2	−1.271 699 99	4.852 265 71	0.501 112 94	−4.251 380 41	0.026 855 76
3	1.240 995 36	−7.066 028 40	−0.094 964 32	2.917 160 94	−0.017 771 26
4	−0.040 504 43	2.369 352 55	−0.325 902 03	0.949 944 70	−0.006 261 21
5	0.020 537 37	−0.036 346 51	−0.022 290 12	0.105 375 29	−0.000 620 62
6	−0.317 633 37	1.258 608 37	0.233 976 66	−1.696 898 74	0.009 809 99
7	−0.714 396 86	2.754 419 01	0.302 234 87	−2.609 771 81	0.016 311 75
8	0.011 700 02	−1.265 717 09	0.131 138 18	−0.272 155 67	0.001 825 00
9	0.001 489 18	−0.002 305 36	−0.001 626 03	0.007 878 55	−0.000 046 27
10	−0.144 514 97	0.156 339 27	0.083 784 65	−0.479 338 27	0.002 861 76
11	−0.139 063 64	1.795 352 31	−0.091 478 04	−0.182 171 32	0.001 114 59
12	0.010 767 56	0.369 604 37	−0.015 815 18	−0.040 679 72	0.000 174 25
13	0.493 978 45	−5.457 948 74	0.268 343 09	0.541 471 94	−0.003 595 93
14	−0.005 673 81	−0.766 516 36	0.032 516 42	0.084 044 06	−0.000 353 39
15	−0.537 419 01	5.353 504 36	−0.256 794 83	−0.519 184 14	0.003 633 00
16	−0.005 093 78	0.396 909 27	−0.016 701 22	−0.043 364 52	0.000 179 15
17	0.182 503 66	−1.689 356 85	0.079 930 54	0.159 579 88	−0.001 151 64

$$f_{gg}^{(22)} = \frac{1}{(16\pi^2)^2} f_{gg}^{(0)}[1152\ln^2\beta + (-2568 + 2304\ln 2)\ln\beta - 79.743\,121\,40] + \frac{n_f}{(16\pi^2)^2} f_{gg}^{(0)}[16\ln\beta - 16 + 16\ln 2] + h(\beta, b_i + n_f c_i), \quad \text{(A6)}$$

where all threshold logarithms $\ln(\beta)$ and the Coulomb corrections ($\sim 1/\beta$) are exact. The fit functions are given in Eqs. (A7)–(A9) and all parameters of the fit are listed in Tables V, VI, and VII. The fits to the scaling functions $f_{ij}^{(21)}$, $f_{ij}^{(22)}$ in Eqs. (A1)–(A6) are, in general, accurate at the per mille level. Exceptions are regions close to zero, which is not surprising. There we retain an accuracy better than 1%.

FORTRAN subroutines with the parametrizations of all scaling functions and the coefficient in Tables V, VI, and VII are available from the authors upon request.

TABLE VI. Coefficients for fits of the gq scaling functions.

	$f_{gq}^{(10)}$	$f_{gq}^{(21)}$		$f_{gq}^{(22)}$	
i	a_i	b_i	c_i	b_i	c_i
1	−0.261 039 70	−0.001 205 32	0.000 032 57	−0.000 222 47	0.000 017 89
2	0.301 926 72	−0.049 063 53	0.000 142 76	0.000 504 22	0.000 000 71
3	−0.015 054 87	−0.208 857 25	−0.004 020 17	−0.029 455 04	−0.000 205 81
4	−0.001 421 50	−13.731 372 24	0.063 298 31	0.343 404 12	0.001 087 59
5	−0.046 606 99	14.018 188 40	−0.059 528 25	−0.318 949 17	−0.000 862 84
6	−0.150 890 38	−0.009 304 88	0.000 026 94	0.000 092 13	0.000 000 10
7	−0.253 977 61	−0.522 236 68	0.001 598 04	0.006 904 02	0.000 016 38
8	−0.009 991 29	−4.684 405 15	0.015 226 72	0.078 472 33	0.000 227 30
9	0.398 787 17	−7.610 461 66	0.028 694 38	0.160 420 51	0.000 456 98
10	−0.024 441 72	1.366 877 43	−0.008 755 89	−0.051 869 74	−0.000 256 20
11	−0.141 783 46	1.846 982 91	−0.008 002 71	−0.038 610 21	−0.000 160 26
12	0.018 672 87	−7.262 659 88	0.040 434 79	0.216 503 62	0.000 707 13
13	0.002 386 56	−4.893 640 26	0.019 658 78	0.101 376 56	0.000 349 37
14	−0.000 033 99	11.045 667 84	−0.052 622 93	−0.280 562 64	−0.000 725 47
15	−0.000 000 89	4.136 601 90	−0.014 573 95	−0.080 904 69	−0.000 255 25
16	0.000 000 00	−6.334 770 51	0.023 146 16	0.130 778 89	0.000 340 15
17	0.000 000 00	−1.089 954 40	0.002 917 92	0.018 138 62	0.000 066 13
18	0.000 000 00	1.190 105 61	−0.002 201 15	−0.015 857 57	−0.000 065 62

TABLE VII. Coefficients for fits of the gg scaling functions.

	$f_{gg}^{(10)}$	$f_{gg}^{(21)}$		$f_{gg}^{(22)}$	
i	a_i	b_i	c_i	b_i	c_i
1	−8.925 632 22	−4.189 314 64	0.123 067 72	0.012 227 83	−0.003 803 86
2	149.905 728 30	82.350 664 06	−2.758 088 06	−0.778 561 84	0.087 577 66
3	−140.556 014 20	−87.873 119 69	3.197 392 72	1.339 556 98	−0.107 422 67
4	−0.341 156 15	9.802 593 28	−0.562 330 45	−0.591 084 09	0.023 827 06
5	−2.410 498 33	−1.122 685 50	0.032 400 48	0.002 483 33	−0.000 997 60
6	54.733 818 89	29.518 302 25	−0.925 417 88	−0.238 272 13	0.029 329 41
7	90.915 480 15	48.361 106 94	−1.571 547 12	−0.388 689 10	0.049 061 47
8	−4.884 010 08	−7.062 617 70	0.351 097 60	0.283 421 53	−0.013 737 34
9	−0.174 667 79	−0.080 252 26	0.002 279 36	0.000 108 76	−0.000 069 86
10	13.470 336 28	7.014 937 79	−0.210 301 53	−0.033 838 62	0.006 583 71
11	22.664 827 10	15.005 881 40	−0.636 884 07	−0.290 710 16	0.020 893 21
12	4.607 266 82	3.841 424 41	−0.129 597 76	−0.114 736 54	0.004 954 14
13	−67.623 423 28	−47.021 617 89	1.916 902 16	0.989 293 69	−0.065 534 59
14	−9.703 914 27	−8.055 833 79	0.267 557 47	0.248 990 69	−0.010 466 35
15	65.080 508 88	47.027 405 35	−1.861 544 23	−1.060 963 21	0.065 591 30
16	5.096 632 60	4.214 380 52	−0.137 958 65	−0.134 253 38	0.005 512 18
17	−20.122 253 41	−14.995 997 32	0.581 550 56	0.359 356 60	−0.020 950 59

$$h(\beta, a_1, \ldots, a_{17}) = a_1\beta^2 + a_2\beta^3 + a_3\beta^4 + a_4\beta^5 + a_5\beta^2\ln\beta + a_6\beta^3\ln\beta + a_7\beta^4\ln\beta + a_8\beta^5\ln\beta + a_9\beta^2\ln^2\beta + a_{10}\beta^3\ln^2\beta + a_{11}\beta\ln\rho + a_{12}\beta\ln^2\rho + a_{13}\beta^2\ln\rho + a_{14}\beta^2\ln^2\rho + a_{15}\beta^3\ln\rho + a_{16}\beta^3\ln^2\rho + a_{17}\beta^4\ln\rho, \tag{A7}$$

$$h_{gq}^{(a)}(\beta, a_1, \ldots, a_{15}) = a_1\beta^4 + a_2\beta^5 + a_3\beta^6 + a_4\beta^4\ln\beta + a_5\beta^5\ln\beta + a_6\beta^6\ln\beta + a_7\beta^2\rho\ln\rho + a_8\beta^2\rho\ln^2\rho + a_9\beta^3\rho\ln\rho + a_{10}\beta^3\rho\ln^2\rho + a_{11}\beta^4\rho\ln\rho + a_{12}\beta^4\rho\ln^2\rho + a_{13}\beta^2\rho\ln^3\rho + a_{14}\beta^2\rho\ln^4\rho + a_{15}\beta^2\rho\ln^5\rho, \tag{A8}$$

$$h_{gq}^{(b)}(\beta, a_1, \ldots, a_{18}) = a_1\beta^3 + a_2\beta^4 + a_3\beta^5 + a_4\beta^6 + a_5\beta^7 + a_6\beta^4\ln\beta + a_7\beta^5\ln\beta + a_8\beta^6\ln\beta + a_9\beta^7\ln\beta + a_{10}\beta^3\ln\rho + a_{11}\beta^3\ln^2\rho + a_{12}\beta^4\ln\rho + a_{13}\beta^4\ln^2\rho + a_{14}\beta^5\ln\rho + a_{15}\beta^5\ln^2\rho + a_{16}\beta^6\ln\rho + a_{17}\beta^6\ln^2\rho + a_{18}\beta^7\ln\rho. \tag{A9}$$

[1] W. Bernreuther, J. Phys. G **35**, 083001 (2008).
[2] J. R. Incandela *et al.*, arXiv:0904.2499.
[3] S. Moch and P. Uwer, Phys. Rev. D **78**, 034003 (2008).
[4] S. Moch and P. Uwer, Nucl. Phys. B, Proc. Suppl. **183**, 75 (2008).
[5] N. Kidonakis and R. Vogt, Phys. Rev. D **78**, 074005 (2008).
[6] M. Cacciari *et al.*, J. High Energy Phys. 09 (2008) 127.
[7] P. M. Nadolsky *et al.*, Phys. Rev. D **78**, 013004 (2008).
[8] V. M. Abazov *et al.* (D0 Collaboration), arXiv:0903.5525.
[9] P. Nason, S. Dawson, and R. K. Ellis, Nucl. Phys. **B303**, 607 (1988).
[10] W. Beenakker *et al.*, Phys. Rev. D **40**, 54 (1989).
[11] W. Bernreuther *et al.*, Nucl. Phys. **B690**, 81 (2004).
[12] M. Czakon and A. Mitov, arXiv:0811.4119.
[13] Tevatron Electroweak Working Group, arXiv:0903.2503.
[14] A. D. Martin *et al.*, arXiv:0901.0002.
[15] N. Kidonakis *et al.*, Phys. Rev. D **64**, 114001 (2001).
[16] M. Cacciari *et al.*, J. High Energy Phys. 04 (2004) 068.
[17] A. Petrelli *et al.*, Nucl. Phys. **B514**, 245 (1998).
[18] K. Hagiwara, Y. Sumino, and H. Yokoya, Phys. Lett. B **666**, 71 (2008).
[19] Y. Kiyo *et al.*, Eur. Phys. J. C **60**, 375 (2009).
[20] W. Beenakker *et al.*, Nucl. Phys. **B411**, 343 (1994).
[21] W. Bernreuther, M. Fücker, and Z. G. Si, Phys. Rev. D **74**, 113005 (2006).
[22] J. H. Kühn, A. Scharf, and P. Uwer, Eur. Phys. J. C **51**, 37 (2007).

[23] N. Gray *et al.*, Z. Phys. C **48**, 673 (1990).
[24] K. G. Chetyrkin and M. Steinhauser, Nucl. Phys. **B573**, 617 (2000).
[25] K. Melnikov and T. v. Ritbergen, Phys. Lett. B **482**, 99 (2000).
[26] E. Laenen, L. Magnea, and G. Stavenga, Phys. Lett. B **669**, 173 (2008).
[27] S. Moch and A. Vogt, J. High Energy Phys. 04 (2009) 081.
[28] S. Moch, J. A. M. Vermaseren, and A. Vogt, Nucl. Phys. **B688**, 101 (2004).
[29] A. Vogt, S. Moch, and J. A. M. Vermaseren, Nucl. Phys. **B691**, 129 (2004).
[30] M. Czakon, A. Mitov, and S. Moch, Nucl. Phys. **B798**, 210 (2008).
[31] M. Czakon, A. Mitov, and S. Moch, Phys. Lett. B **651**, 147 (2007).
[32] J. G. Körner, Z. Merebashvili, and M. Rogal, Phys. Rev. D **77**, 094011 (2008).
[33] B. Kniehl *et al.*, Phys. Rev. D **78**, 094013 (2008).
[34] C. Anastasiou and S. M. Aybat, Phys. Rev. D **78**, 114006 (2008).
[35] R. Bonciani *et al.*, arXiv:0810.0598.
[36] M. Czakon, Phys. Lett. B **664**, 307 (2008).
[37] R. Bonciani *et al.*, arXiv:0906.3671.
[38] R. Bonciani *et al.*, Nucl. Phys. **B529**, 424 (1998).
[39] S. Dittmaier, P. Uwer, and S. Weinzierl, Phys. Rev. Lett. **98**, 262002 (2007).
[40] S. Dittmaier, P. Uwer, and S. Weinzierl, Eur. Phys. J. C **59**, 625 (2009).
[41] A. H. Hoang *et al.*, Eur. Phys. J. direct C **2**, 1 (2000).
[42] G. Rodrigo, A. Santamaria, and M. S. Bilenky, Phys. Rev. Lett. **79**, 193 (1997).
[43] A. Brandenburg *et al.*, Phys. Lett. B **468**, 168 (1999).
[44] R. Barate *et al.* (ALEPH Collaboration), Eur. Phys. J. C **18**, 1 (2000).
[45] G. Abbiendi *et al.* (OPAL Collaboration), Eur. Phys. J. C **21**, 411 (2001).
[46] J. Abdallah *et al.* (DELPHI Collaboration), Eur. Phys. J. C **46**, 569 (2006).
[47] J. Abdallah *et al.* (DELPHI Collaboration), Eur. Phys. J. C **55**, 525 (2008).
[48] A. H. Hoang *et al.*, Phys. Rev. Lett. **101**, 151602 (2008).